Effects of the bottom slope and guiding wall length on the performance of a vortex drop inlet

Rhee, Dong Sop; Park, Yong Sung; Park, Inhwan

Published in:
Water Science and Technology

DOI:
10.2166/wst.2018.397

Publication date:
2018

Document Version
Peer reviewed version

Effects of the bottom slope and guiding wall length on the performance of a vortex drop inlet

Dong Sop Rhee

Principal Researcher, Korea Institute of Construction Technology, 283 Goyangdae-Ro, Ilsanseo-Gu, Goyang-Si, Gyeonggi-Do, 10223, Republic of Korea. E-mail: dsrhee@kict.re.kr

Yong Sung Park

Senior Lecturer & Royal Society of Edinburgh/Scottish Government Personal Research Fellow Co-Funded by the Marie-Curie Actions, School of Science & Engineering, University of Dundee, Dundee DD1 4HN, UK. E-mail: y.s.park@dundee.ac.uk

Inhwan Park

Cooresponding author, Post-doctoral Researcher, Korea Institute of Construction Technology, 283 Goyangdae-Ro, Ilsanseo-Gu, Goyang-Si, Gyeonggi-Do, 10223, Republic of Korea. E-mail: inhwanpark@kict.re.kr

Abstract

Laboratory experiments were conducted to assess the performance of a vortex drop inlet with a spiral intake. The water surface elevation at multiple locations was measured for different flowrates by varying the extent of the guiding wall and the longitudinal and radial bottom slopes. The measurements show that a steeper longitudinal bottom slope decreases the water surface elevation at the beginning of the intake, resulting in a transcritical flow in the intake structure. However, a steeper longitudinal bottom slope also causes the maximum water surface elevation to occur within the spiral intake. For an effective vortex drop inlet design, achieving a low water surface elevation throughout the entire spiral intake structure is required. Experimental results show that the two seemingly conflicting design criteria, namely, achieving a low water surface elevation in the approach channel and reducing the maximum water surface elevation in the intake structure, can be simultaneously achieved by adding a radial bottom

slope.

Keywords: choking, guiding wall, longitudinal bottom slope, raidial bottom slope, vortex drop inlet

Introduction

The types of manholes can be classified as plunging flow drops and vortex drops (Jain 1984). As the name implies, in a vortex drop, the flow enters through the approach channel and forms a vortex or spiral along the circular wall of the shaft as it travels downward; in a plunging flow drop, a jet flow occurs (Rajaratnam et al. 1997; Banisoltan et al. 2015). The vortex flow in the vertical shaft leads to entrain air, which pushes down odors to the underground space (Motzet & Valentin 2002) and to dissipate flow energy by friction while flowing down the wall of the vertical shaft (Zhao et al. 2006; Del Giudice et al. 2010). For these reasons, vortex drops are preferred in the aspects of efficient conveyance and significant energy dissipation (Hager 1985). In general, the inlet of the vertical shaft can have a screw (Drioli 1947), tangential (Jain & Kennedy 1983), or spiral (Kellenberger 1988) shape, based on the properties of the approaching flow (see Appendix 1). However, despite the advantages of vortex drops, they have a relatively high cost due to geometrical complexities, and possible flow patterns disturbing stable flow conveyance (e.g., standing wave and choking in the intake structure) are obstacles to using vortex drops. Therefore, reasonable design guidelines to increase the efficiency of vortex drops are necessary.

The flow properties in the intake structure of vortex drops have been studied for optimal design. For the case of a spiral inlet, Quick (1990) published a study of head-discharge relationships to find an efficient design for intake structures. Hager (1990) reported a theoretical formula for the free surface profile of a standing wave along the intake wall for a supercritical approaching flow. In consideration of the relatively high cost of a spiral inlet, Motzet & Valentin (2002) tested a supercritical flow in a screw shaped intake structure, which was originally intended to convey a subcritical flow, and concluded that the screw inlet could still be used in the case of a supercritical approaching flow, although the energy dissipation decreases. Subsequently, Del Giudice et al. (2010) and Del Giudice & Gisonni (2011) proposed a new design criterion for the screw intake structure to be applied in both in subcritical and supercritical flows. Furthermore, Mulligan et al. (2016) presented an empirical formula for

the discharge in a strong free-surface vortex flow to design a screw intake structure. Previous experimental studies were primarily focused on screw or tangential intake structures for a subcritical approaching flow. However, in many situations, a supercritical flow commonly occurs at the entrance of the vertical shaft. Thus, the geometry for the vortex drop shaft with a spiral intake must be tested under several design conditions.

The primary objective of the inlet is to achieve a high-volume flow rate with a minimal increase in the upstream water depth. However, there are at least two important factors to be considered in designing and evaluating the efficiency of a vortex drop inlet. One factor is the possibility of choking leaving no space for air to escape. Choking often results in a significant decrease in conveyance and explosive bursts of air, with associated safety issues; therefore, a vortex drop inlet must be designed such that choking events are prevented. To ensure that there is adequate passage for air flow at the centre of the vertical shaft, especially for a supercritical approaching flow, an intake structure consisting of a steep channel with an inner guiding wall could be fitted near the entrance of the vertical shaft. In addition, it is well-known that a standing wave can form during high-speed flow in a curved channel (e.g. Ippen, 1943); therefore, the maximum water surface elevation may occur at the crest of a standing wave located within the inlet structure (Wu et al. 2017). This possibility is the other factor to be considered in the design of an inlet structure. Based on physical model tests, Hager (1990; 2010) provided a guideline for the inlet structure geometries, optimizing the height of the standing wave and preventing choking for approaching flows with a high Froude number.

In the present research, we build upon the guidelines for spiral intake structures in conditions of subcritical and transcritical flows and further investigate the effects of the bottom slope and the guiding wall. In particular, two types of bottom slope configurations are used: (i) longitudinal slope only and (ii) both longitudinal and radial slopes. For both types, the length of the inner guiding wall was varied, and the performance was assessed in terms of the water surface elevation at the junction between the approach channel and the vertical shaft as well as in terms of the height of the standing wave, if a standing wave occurred. It is shown that a radial slope effectively eliminates the standing wave, even for a large flow rate.

Methods

We focus on the spiral vortex drop, which is designed for a supercritical flow, and additional design

parameters are investigated for subcritical and transcritical approach flows. For the design of the vortex drop intake, Hager (1990; 2010) recommended the design parameters as shown in Appendix 1(b), where R_1, R_2, R_3, and R_4 are the radii of the inlet structure; R is the radius of the vertical shaft; a is the horizontal distance from the outer wall of the approach channel to the centre of the vertical shaft; b is the width of the approach channel; d is the width of the channel opposite the inlet section; and s is the thickness of the wall opposite the inlet section; s_1 is the thickness of the inlet section; e_1, e_2, e_3, and e_4 are the eccentricities of the circular arc constituting the inlet structure; S_{oo} is the bottom slope of the spiral intake.

As mentioned in the previous section, the maximum water surface elevation measured from the start of the spiral intake, h_M, may occur within the intake structure because of the standing wave. An empirical equation for h_M in terms of the inlet geometric parameters and discharge was given by Hager (1990; 2010) who derived the equation for supercritical flow as follows:

$$\frac{h_M}{R_1} = \left[\left(\frac{2}{g b h_0 R_1^3} \right)^{1/2} Q - \frac{1}{2} S_{oo} \right] \left(1.1 + 0.15 F_0 \right) \tag{1}$$

in which Q is the discharge, g is the gravitational acceleration, h_0 is the water depth at the start of the intake, and F_0 is the Froude number at the same location defined as

$$F_0 = \frac{Q}{\sqrt{g b^2 h_0^3}} \tag{2}$$

The design of inlet structure should be determined to minimize h_M for the efficient drainage of stormwater. In this study, h_M was measured for both longitudinal and radial slopes.

Experiments were conducted at the River Hydraulics Laboratory of the Korea Institute of Civil Engineering and Building Technology (KICT). The experimental apparatus is depicted in Figure 1, in which the approach

channel (0.6 m long, 0.2 m wide, 0.6 m high) and the vertical shaft with a spiral intake structure ($a = 0.30$ m, $s = 0.01$ m, $d = 0.10$ m, $R_1 = 0.25$ m, $R_2 = 0.15$ m, $R_3 = 0.09$ m, $R_4 = 0.10$ m, and $R = 0.09$ m) were built of clear acrylic. Flow was supplied from the high-elevation tank at the beginning of the approach channel. The discharged water is eventually collected at the basin underneath the vertical shaft and then recirculated through a submerged pump. The spiral intake structure was designed according to the design criteria presented by Hager (1990; 2010) who proposed the design parameters for a supercritical flow. Figure 1b) shows the details of the intake structure, in which the spiral inlet has the longitudinal (S_{oo}) and radial bottom slopes (S_{oe}). In this channel, S_{oo} and S_{oe} were changed to assess the drainage efficiency in conditions of subcritical and transcritical flows. Furthermore, the length of the guiding wall was maniputated by varying the angle, θ.

Figure 1 Descriptions of the experimental apparatus

A total of six different intake structures were built with different bottom slope configurations of the spiral intake. Four of the structures had only longitudinal slopes ($S_{oo} = 5.0\%$, 7.5%, 10.0%, and 12.5%), and the other two had both longitudinal and radial slopes ($S_{oo} = 5\%$ and 10% with $S_{oe} = 5\%$). For each of the six spiral intakes, the water surface elevation was measured at each measurement sections as shown in Figure 1b) using both a capacitance-type wave gauge, which has $\pm 0.3\%$ error, and tape rulers attached to the vertical shaft (see Appendix 2). For each spiral intake with different bottom slopes, measurements were repeated as varying the length of the guiding wall (θ = 0°, 30°, 60°, 90°, 120°, 150°, 180°, 210° and 270°). In this experimental apparatus, discharge ($0.002 \le Q \le 0.030\,\mathrm{m}^3/\mathrm{s}$) was varied and the flow changed from the weakly subcritical to the transitional flow ($0.117 \le F_0 \le 1.247$) according to the hydraulic and geometric conditions. The aforementioned experimental conditions are listed in Table 1.

Table 1 Summary of the experimental conditions

Results and discussion

In this section, we present three sets of analysed data that are directly relevant to the performance of the vortex drop inlet: (i) water surface elevation–discharge relations, i.e., h_0 as a function of Q for each case; (ii) h_M/h_0 as a function of Q for each case; and (iii) F_0 as a function of Q for each case. Additionally, we remark here that both h_0 and Q are expressed in terms of dimensionless variables defined as follows (Hager 1990; Hager 2010):

$$y = \frac{bh_0}{aR} \tag{3}$$

$$q = Q\sqrt{\frac{b}{gaR^5}} \tag{4}$$

Water surface elevation change by bottom slopes

Figure 2 shows the water surface elevation changes observed along the inside of the intake structure. The figure reveals that the water surface elevation (h) rises with increasing discharge (Q). In Figure 2a), which shows the results for only a longitudinal bottom slope ($S_{oo} = 10\%$), standing waves are clearly visible (section no. 2-4) and result in 9.9%-38.9% higher water surface elevation (h_M) within the intake structure where is between the section no. 2 and no. 4 than the water surface elevation at the beginning of the inlet (h_0). Furthermore, two local maximum water surface elevations were observed as reported by Hager (1990) and Crispino et al. (2016) in conditions of supercritical flow even though the hydraulic conditions in this measurements show subcritical and transcritical flows. After that, the local maximum water surface elevation was reduced along the spiral inlet due to subcritical and transcritical inflow conditions. In contrast, in Figure 2b), h_M is only 0.1%-0.7% higher than h_0 in subcritical flow even though h_M is located at the section no. 2. In conditions of transcritical flow, h_0 is higher than the water surface elevation in the inlet structure except the results for $F_0 = 1.088$ in which h_M is 2.6% higher than h_0. These results show that h_M can decrease in the inlet structure by adding radial bottom slope.

Figure 2 Experimental results for water surface elevations measured at intervals from the start of the spiral intake

The dimensionless water surface elevation at the beginning of the spiral intake (y) is plotted as a function of the dimensionless discharge (q) for varying longitudinal bottom slopes (S_{oo}) in Figure 3. The dimensionless critical depth, which is calculated by replacing h_0 to the critical depth, is also plotted in Figure 3 using a dashed line. For all cases, the guiding wall managed to prevent choking in the vertical shaft. However, as the extent of the guiding wall increases, more space is taken up by the wall, leaving less room for flow. As a result, y increases not only with q but also with θ, which results in a rapid increase of y with increasing q. Furthermore, the flow shown in Figures 3b)-3d) changes from a transcritical to a subcritical flow as increasing q. As the longitudinal bottom slope increases from 5.0% to 10.0% (Figures 3a) – 3c)), the adverse effects of the guiding wall are minimized, and there is a negligible difference between cases with different extents of the guiding wall when the bottom slope is 10.0%. However, for the case with a steeper slope (12.5%, Figure 3d)), the performance deteriorates again. Thus, the results suggest that there exists an optimal longitudinal bottom slope.

Figure 3 y as a function of q for the case with a longitudinal slope

The effects of the radial bottom slope (S_{oe}) can be observed by comparing Figures 3a) and 4a) as well as Figures 3c) and 4b). For the cases with a 5% longitudinal bottom slope, the radial slope (Figure 4a) leads to 0.1%-11.6% decrease over the case without a radial slope (Figure 3a) for $\theta \geq 180°$. In contrast, the effect of the 5% radial bottom slope is significantly improved for the cases with a steeper (10%) longitudinal bottom slope, in which y decreases 11.2%-12.0% for $\theta \geq 180°$.

Figure 4 y as a function of q for cases with longitudinal and radial slopes

The maximum water surface elevation in the inlet structure

177 The maximum water surface elevation in the inlet structure is one of the key parameters in designing vortex
178 drop inlets. As mentioned previously, with the addition of a spiral intake structure and a guiding wall, the maximum
179 water surface elevation may occur downstream from the beginning of the intake even though subcritical or
180 transcritical flows occurred at the sprial inlet. Therefore, the maximum water surface elevation within the spiral
181 intake (h_M) measured from the junction of the inlet channel and the spiral intake relative to the water surface
182 elevation at the junction (h_0) is expressed as a function of q in Figures 5 and 6. For each case, h_M/h_0 increases
183 as the extent of the guiding wall decreases, primarily because h_0 or y increases as the extent of the guiding wall
184 increases, as shown previously in Figure 3. However, h_M/h_0 does not show monotonic behaviour with respect to
185 q , in contrast with the monotonic tendency of y in Figure 3; instead, it either maintains an approximately
186 constant value (Figures 5*a*), 6a) and 6b)) or increases initially and later decreases from a maximum to a constant
187 value (Figures 5b), 5c) and 5d)). Interestingly, in these latter cases, the increased longitudinal bottom slope
188 effectively reduced y . Therefore, it is reiterated once again that h_M is also an important design parameter.
189

Figure 5 h_M / h_0 as a function of q for the case with a longitudinal slope

190

Figure 6 h_M / h_0 as function of q for cases with longitudinal and radial slopes

191

192 This rather complicated behaviour of h_M/h_0 can be explained in terms of the Froude numbers defined in
193 Eq. (14), which are plotted in Figures 7 and 8. First, the two cases with a 5.0% longitudinal bottom slope (Figures 7a)
194 and 8a)) maintain a subcritical flow under all experimental conditions, and the maximum elevation occurs at the
195 beginning of the spiral intake. By comparing Figures 7b), 7c) and 7d) to the corresponding Figures 5b), 5c) and 5d),
196 it is observed that h_M/h_0 is greater than one for subcritical and transcritical flows. With a further increase of q ,
197 the water depth goes beyond the critical value, and the flow becomes subcritical as shown in Figures 3 and 4, while
198 h_M/h_0 decreases to a constant value.
199

Figure 7 F_0 as a function of q for the case with a longitudinal slope

200

Figure 8 F_0 as a function of q for cases with longitudinal and radial slopes

201

202 The experimental result for the spiral intake with both a 10.0% longitudinal bottom slope and a 5.0% radial
203 slope (Figure 8b)) is quite interesting. Except for the case with a 270° guiding wall, which consistently shows a
204 subcritical flow, the flows are, in general, trans-critical. Unlike the previous observation illustrated in Figures 5b), 5c)
205 and 5d), this case maintains $h_M/h_0 \approx 1$ for all discharge conditions, similar to the cases with a subcritical flows,
206 because the radial slope shifts the hydraulic jump further downstream in the spiral intake (see Figure 2). The average
207 values of y and h_M/h_0 ($\bar{y}$ and $\overline{h_M/h_0}$) are compared in Table 2 based on the radial bottom slope. The
208 difference (ε) between the two observations was calculated as follows:

209

210 $$\varepsilon = \frac{1}{n}\sum_{i=1}^{n}\frac{\xi_i - \zeta_i}{\xi_i} \tag{6}$$

211

212 in which ξ_i and ζ_i are the measurements for $S_{oe} = 0\%$ and $S_{oe} = 5\%$, respectively, and n is the number
213 of measurements. The comparisons show that y and h_M/h_0 decrease in all cases with a radial bottom slope.
214 This results is important evidence indicating that, by adding a radial bottom slope, it is possible to meet two
215 seemingly conflicting design criteria, i.e., achieving a low y and low h_M/h_0 at the same time.

216

Table 2 Changes in y and h_M/h_0 according to the radial bottom slope

217

218 **Conclusions**

219

220 In this study, the performance of a spiral inlet, which is designed for a supercritical flow, was investigated
221 experimentally in conditions of subcritical and transcritical flows. To prevent choking in the vertical shaft, a spiral
222 intake structure with a guiding wall was installed. After varying the extent of the guiding wall and the longitudinal

and radial bottom slopes, water surface elevations were measured at a number of positions within the spiral inlet for different discharges. In all cases, choking was successfully prevented. Overall, a steeper longitudinal bottom slope reduces the water surface elevation at the beginning of the intake. However, a steeper bottom slope results in a transcritical flow in the intake structure, which causes the maximum water surface elevation to occur within the spiral intake. For effective design of a spiral inlet in subcritical and transcritical flows, achieving a low water surface elevation throughout the spiral intake structure is necessary; here, we experimentally showed that this can be achieved by using a radial bottom slope. Further work using model experiments and numerical simulations is underway to quantify the optimum design criteria by varying more various bottom slopes.

Acknowledgement

This study was supported by the grant (17CTAP-C095650-03) from Infrastructure and Transportation Technology Promotion Program funded by Ministry of Land, infrastructure, and Transport of Korean government and funded by the project 'Development of Urban Flood Mitigation Technology (Smart Flood Management)' of Korea Institute of Civil Engineering and Building Technology

References

1. Banisoltan S., Rajaratnam N., & Zhu D. Z. 2015 Experimental study of hydraulics of drill-drop manholes. *Journal of Hydraulic Engineering*, **141**(10), 04015021.
2. Crispino G., Dorthe D., Gisonni C., & Pfister M. 2016 Junction chamber at vortex drop shaft: case study of Cossonay. In: *Proceedings of the 6th IAHR Int. Symp. on Hydraul. Struct*, Portland, OR, pp 437-446.
3. Drioli C. 1947 Su un particolare tipo d'imbocco per pozzi di scarico. *L' Energia Elettrica*, **24**, pp. 447-452 (in Italian).
4. Del Giudice G. & Gisonni C. 2011 Vortex dropshaft retrofitting: case of Naples city (Italy). *Journal of Hydraulic Research,* **49** (6), pp. 804-808.
5. Del Giudice G., Gisonni C., & Rasulo G. 2010 Design of a scroll vortex inlet for supercritical approach flow. *Journal of Hydraulic Engineering*, **136** (10), pp. 837-841.
6. Hager W. H. 1985 Head-discharge relation for vortex shaft. *Journal of Hydraulic Engineering*, **111** (6), pp. 1015–1020.

7. Hager W. H. 1990 Vortex drop inlet for supercritical approaching flow. *Journal of Hydraulic Engineering*, **116** (8), pp. 1048–1054.

8. Hager W. H. 2010 *Wastewater Hydraulics*, 2nd ed. Springer.

9. Ippen A. T. 1943 Gas-wave analogies in open channel flow. In: *Proceedings of the 2nd Hydraulic Conference*, Bulletin **27**, Studies in Engineering, University of Iowa.

10. Jain S. C. 1984 Tangential vortex-inlet. *Journal of Hydraulic Engineering*, **110** (12), pp. 1683-1699.

11. Jain S. C. & Kennedy J. F. (1983) Vortex-flow drop structures for the milwaukee metropolitan sewerage district inline storage system. *IIHR Report No. 264*, Iowa Institute Hydraulic Research, University of Iowa, Iowa City, Iowa.

12. Kellenberger M. H. 1988 *Wirbelfallschächte in der Kanalisationstechnik*, Doctoral dissertation, Swiss Federal Institute of Technology, Zurich, Switzerland (in German).

13. Motzet K. M. & Valentin F. 2002 Efficiency of a vortex chamber with horizontal bottom under supercritical flow. *Global Solutions for Urban Drainage*, ASCE, pp. 1-11.

14. Mulligan S., Casserly J., & Sherlock R. 2016 Effects of geometry on strong free-surface vortices in subcritical approach flows. *Journal of Hydraulic Engineering*, **142** (11), 04016051.

15. Rajaratnam N., Mainali A., & Hsung C.Y. 1997 Observations on flow in vertical dropshafts in urban drainage systems. *Journal of Hydraulic Engineering*, **123** (5), pp. 486-491.

16. Quick M. (1990) Analysis of spiral vortex and vertical slot vortex drop shafts. *Journal of Hydraulic Engineering*, **116** (3), pp. 309-325.

17. Wu J., Ren, W., & Ma F. 2017 Standing wave at dropshaft inlets. *Journal of Hydrodynamics*, **29** (3), pp. 524-527.

18. Zhao C.H., Zhu D.Z., Sun S.K., & Liu Z.P. 2006 Experimental study of flow in a vortex drop shaft. *Journal of Hydraulic Engineering*, **132** (1), pp. 61-68.

Table 1 Summary of the experimental conditions

Q (m^3/s)	θ (°)	S_{oe} (%)	S_{oo} (%)	F_o	q
0.002 - 0.025	0 - 270	0.0	5.0	0.117-0.668	0.158-2.030
			7.5	0.137-1.129	
			10.0	0.188-1.129	
			12.5	0.175-1.218	
		5.0	5.0	0.162-1.202	
			10.0	0.207-1.247	

Table 2 Changes in y and h_M/h_0 according to the radial bottom slope

Case		S_{oo} = 5%		ε (%)	S_{oo} = 10%		ε (%)
		S_{oe} = 0%	S_{oe} = 5%		S_{oe} = 0%	S_{oe} = 5%	
$\theta = 210°$	$\bar{y}$	1.18	1.06	0.09	0.68	0.62	11.17
	$\overline{h_M/h_0}$	1.04	1.01	3.94	1.23	1.00	16.04
$\theta = 180°$	$\bar{y}$	0.98	0.83	11.60	0.73	0.58	11.98
	$\overline{h_M/h_0}$	1.05	1.01	5.12	1.25	1.01	17.70
$\theta = 120°$	$\bar{y}$	0.85	0.73	13.99	0.61	0.53	12.17
	$\overline{h_M/h_0}$	1.06	1.01	5.21	1.28	1.00	19.46
$\theta = 90°$	$\bar{y}$	0.71	0.66	17.32	0.58	0.53	6.86
	$\overline{h_M/h_0}$	1.08	1.02	4.54	1.33	1.00	21.03

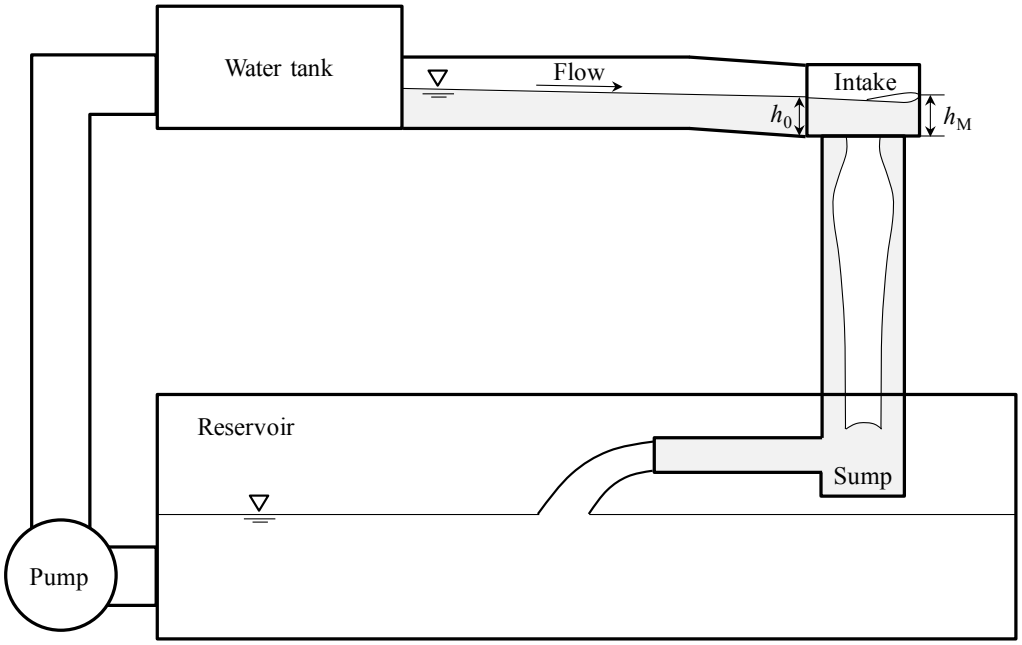

a) Outlines of experimental channel

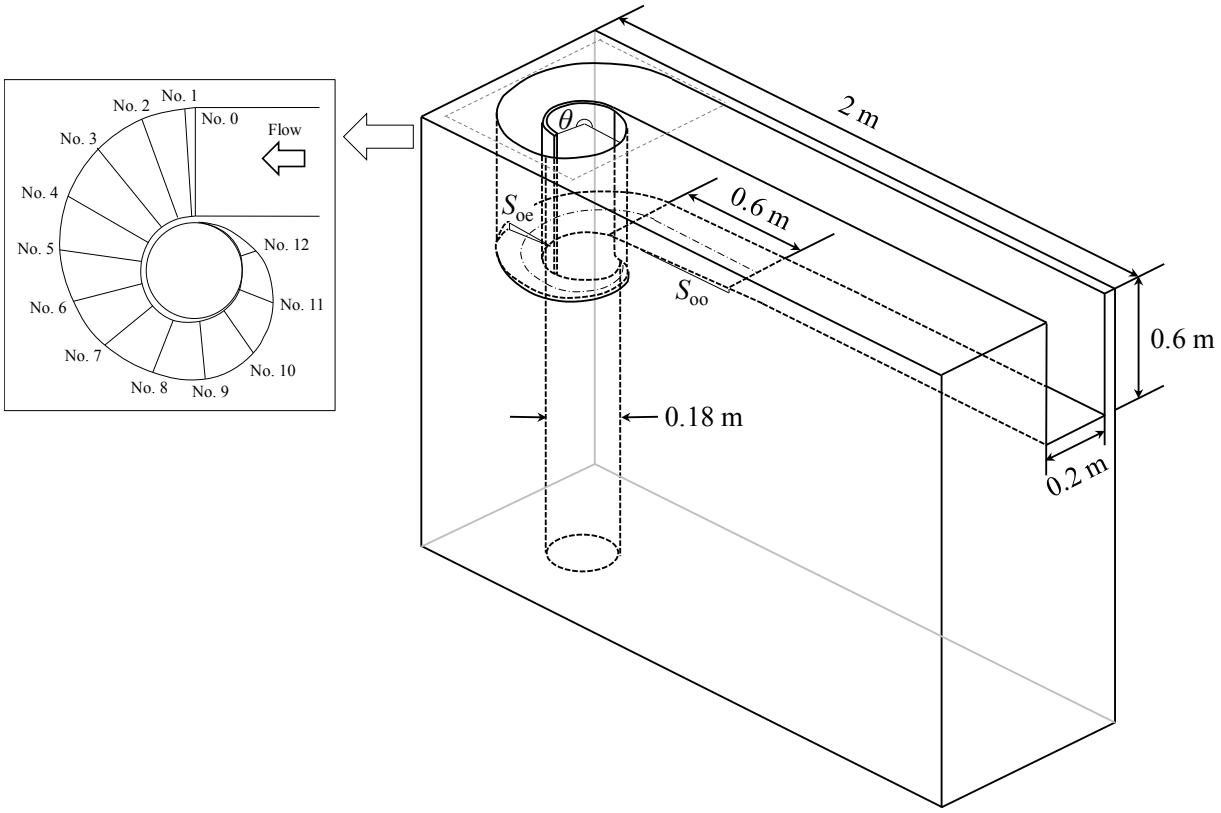

b) Detailes of intake structures and measurement sections

Figure 1 Descriptions of the experimental apparatus

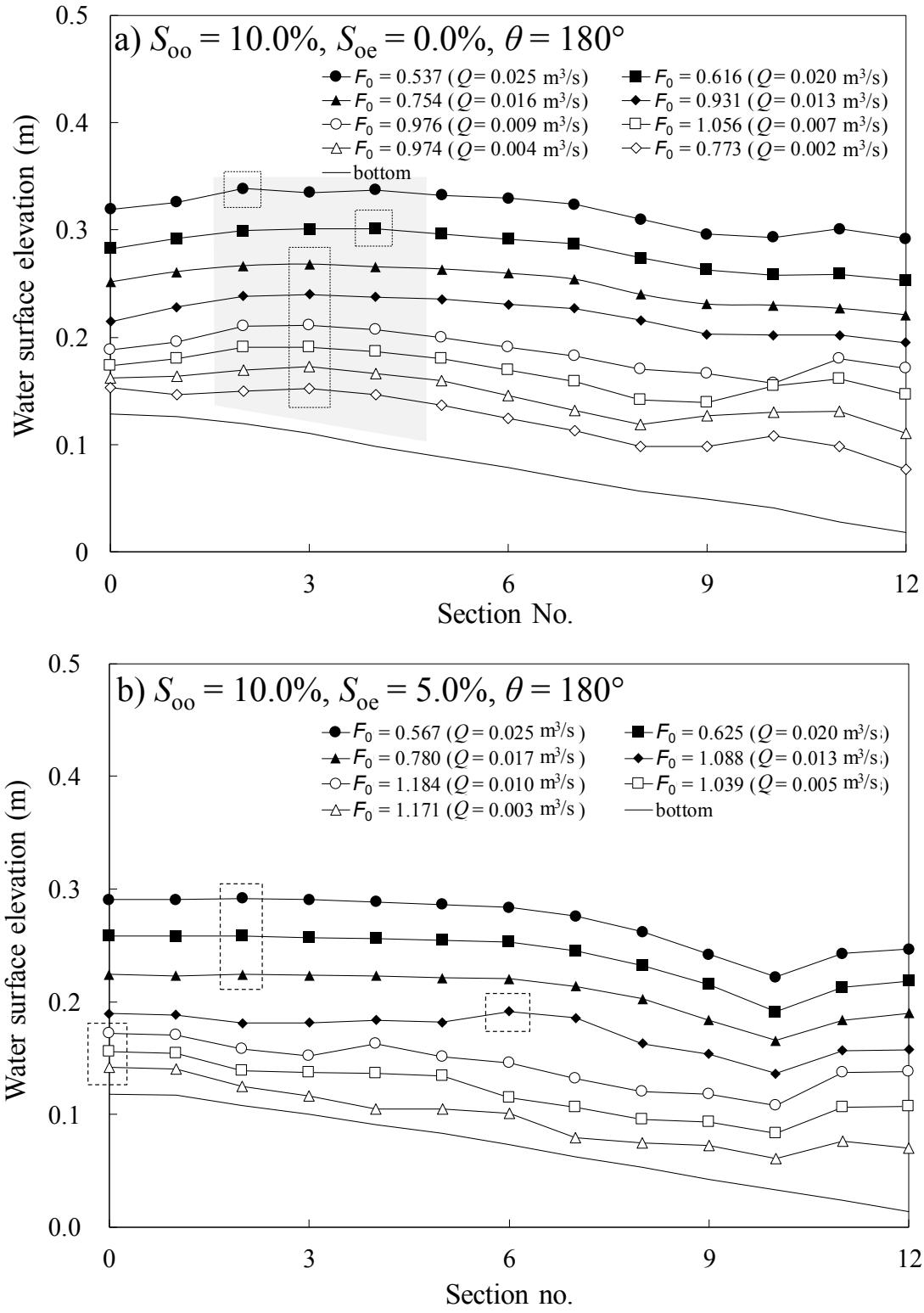

Figure 2 Experimental results for water surface elevations measured at intervals from the start of the spiral intake

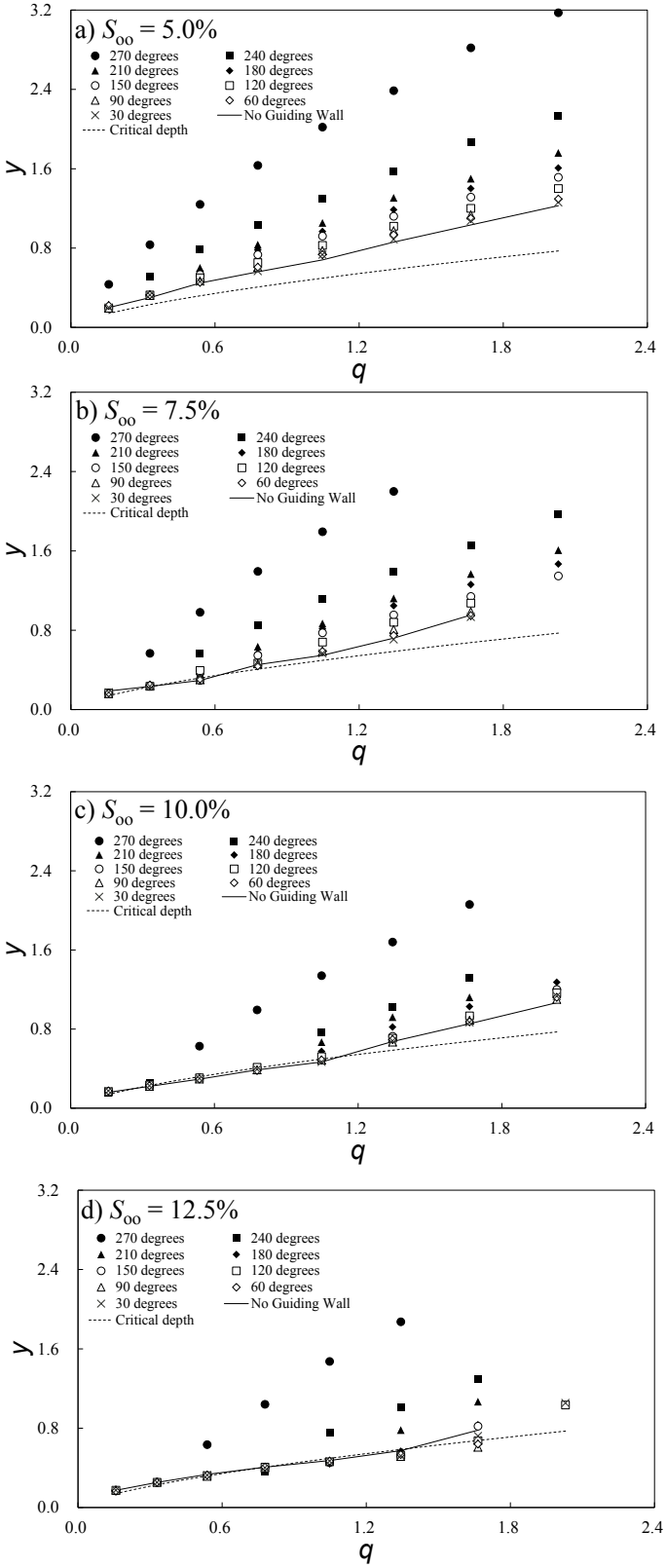

Figure 3 y as function of q for the case with a longitudinal slope

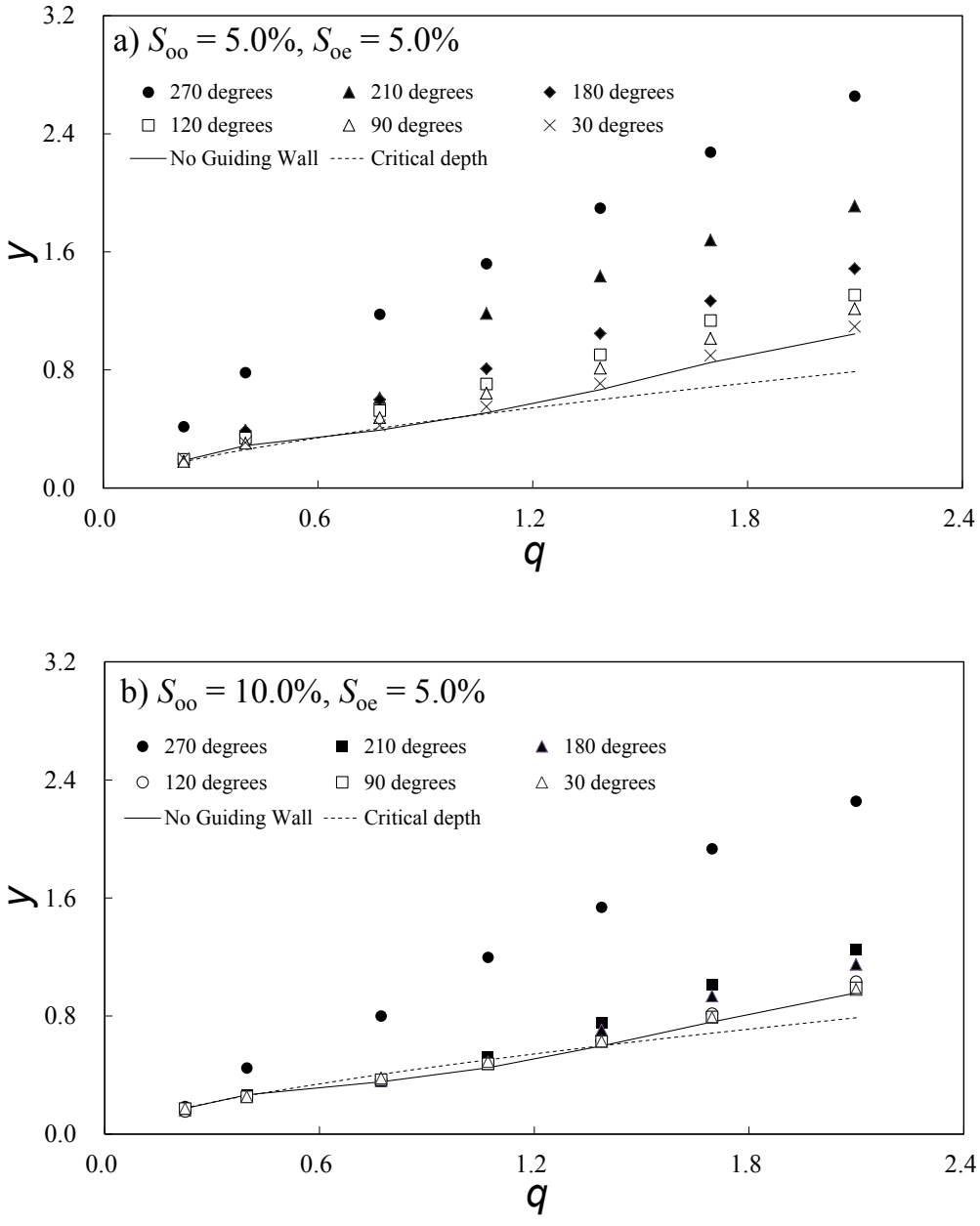

Figure 4 y as a function of q for cases with longitudinal and radial slopes

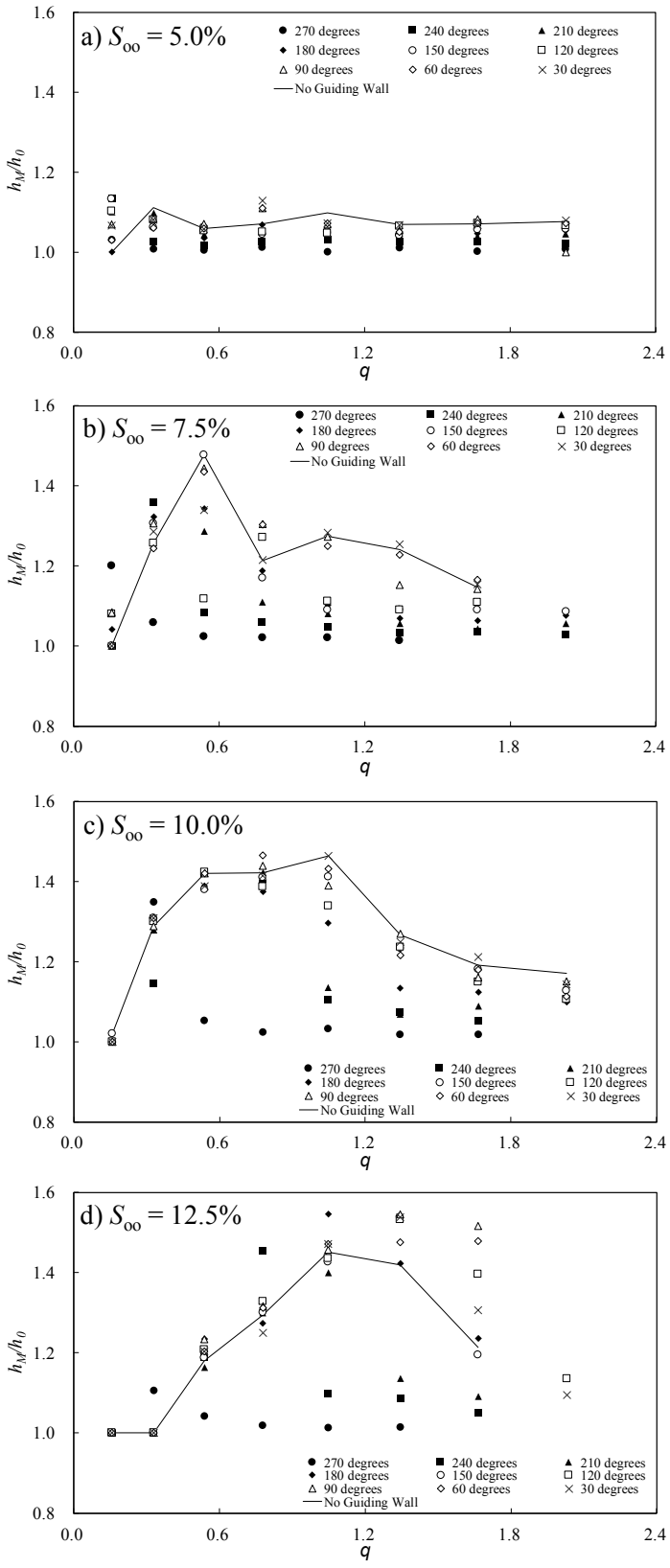

Figure 5 h_M/h_0 as a function of q for case with a longitudinal slope

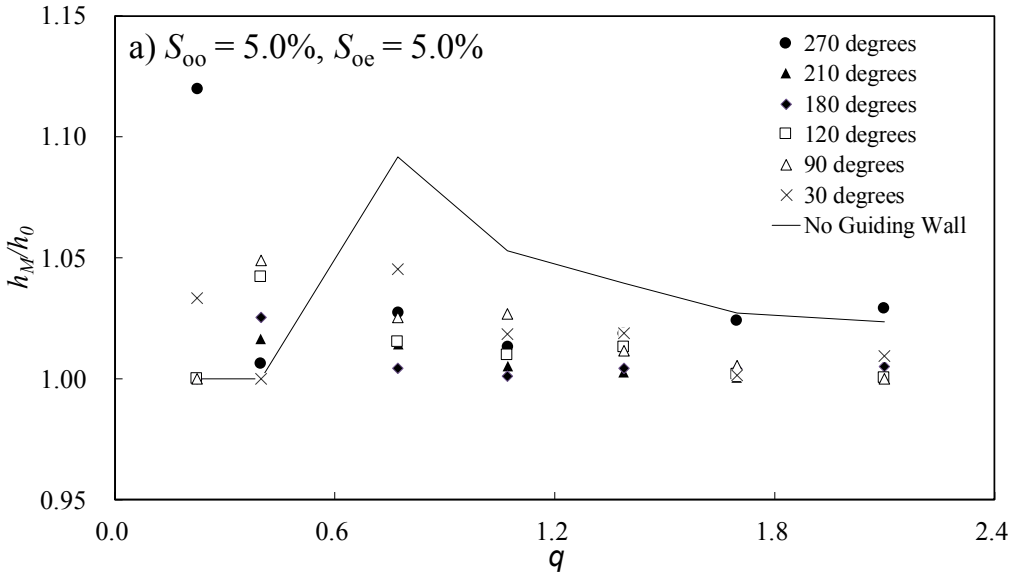

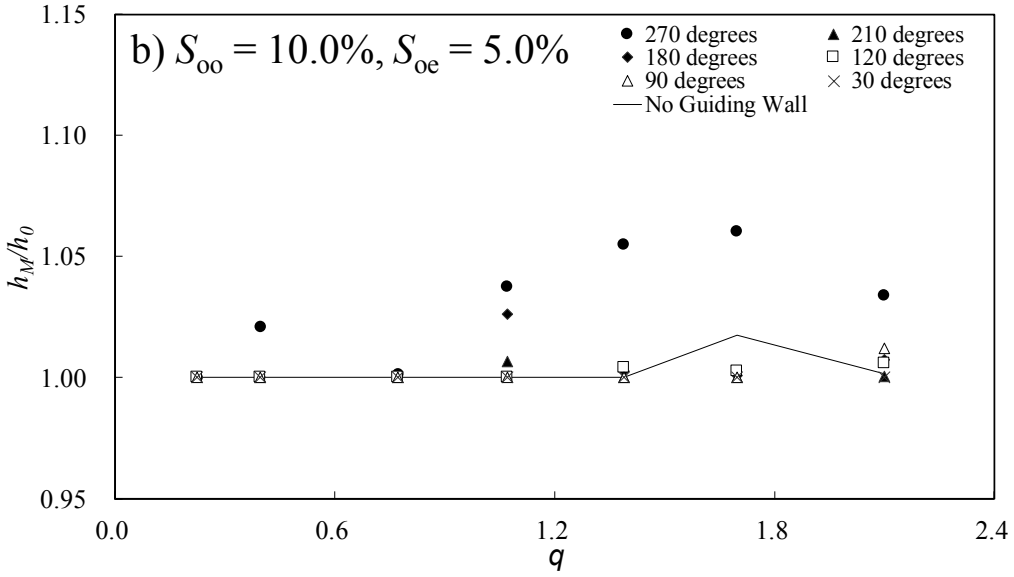

Figure 6 h_M/h_0 as function of q for cases with longitudinal and radial slopes

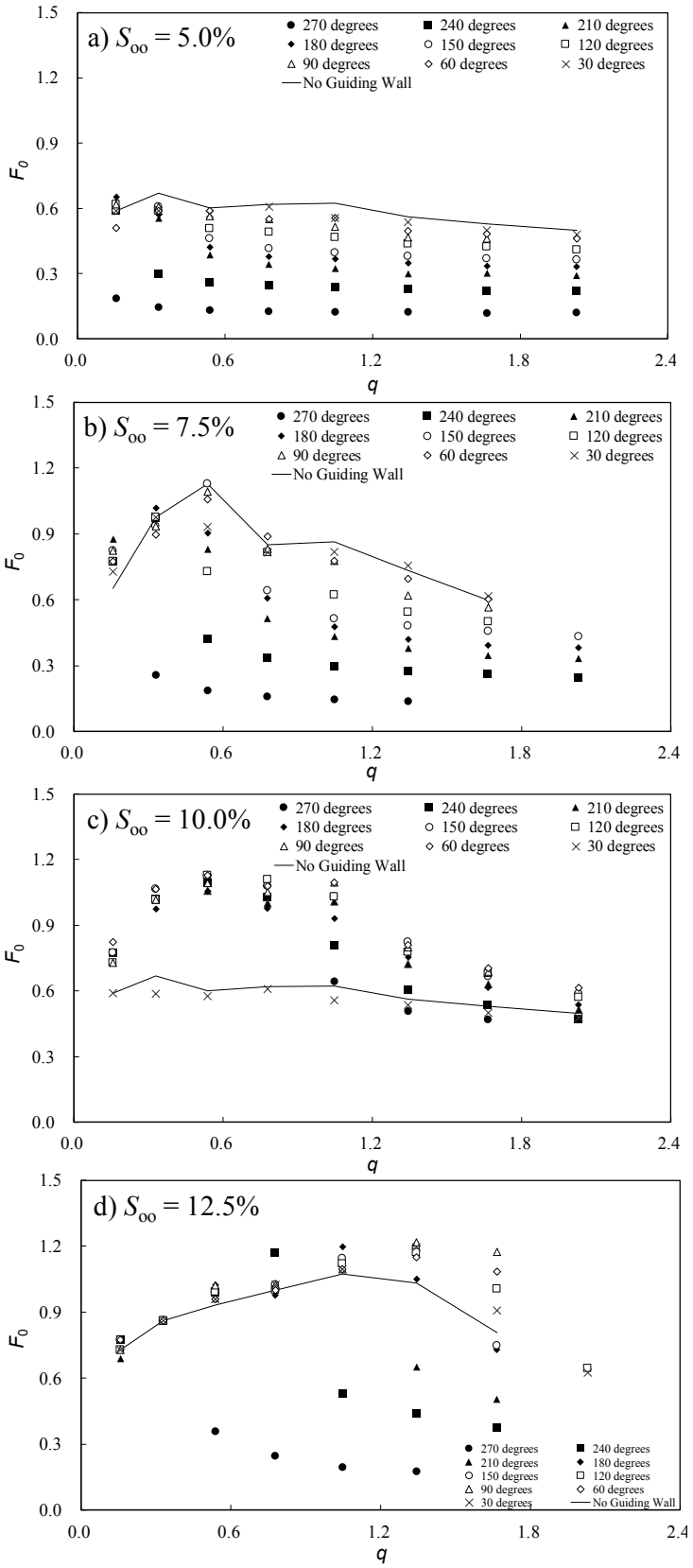

Figure 7 F_0 as a function of q for the case with a longitudinal slope

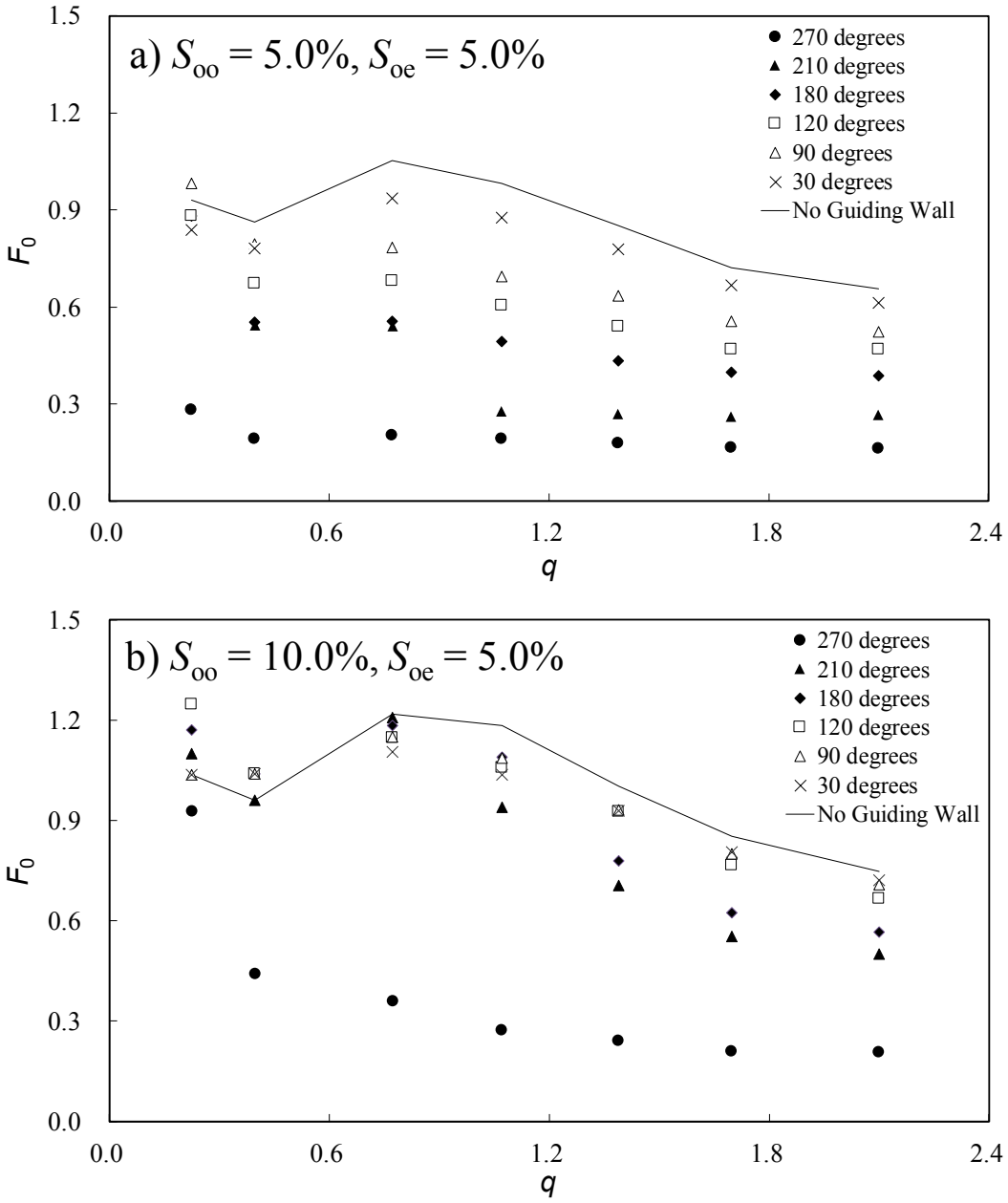

Figure 8 F_0 as a function of q for cases with longitudinal and radial slopes

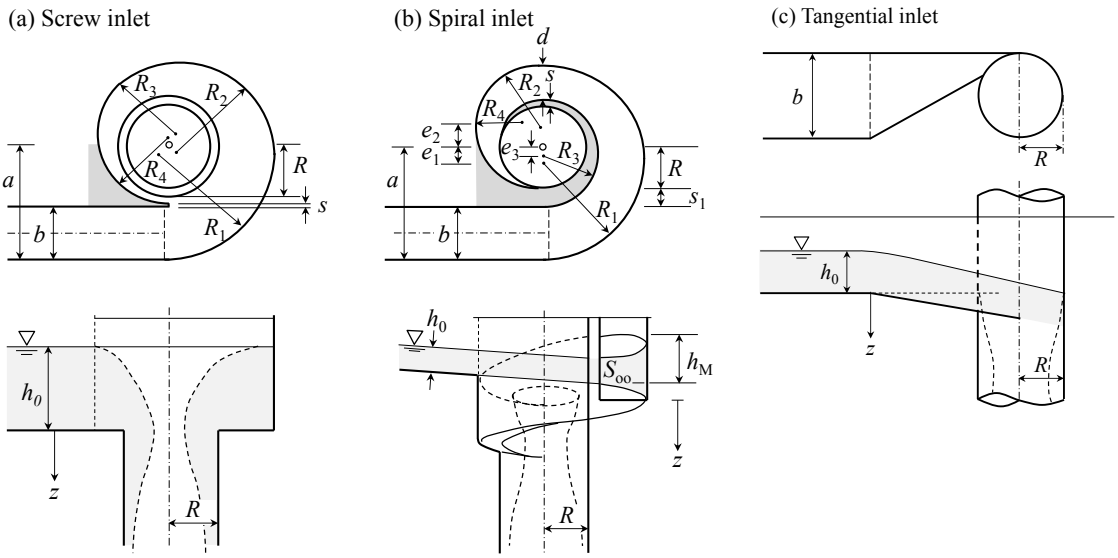

Appendix 1 Schematic diagrams for vortex drop inlets (adapted from Hager, 2010)

(a) Approach channel with the high-elevation tank

(b) Vertical shaft and outlet

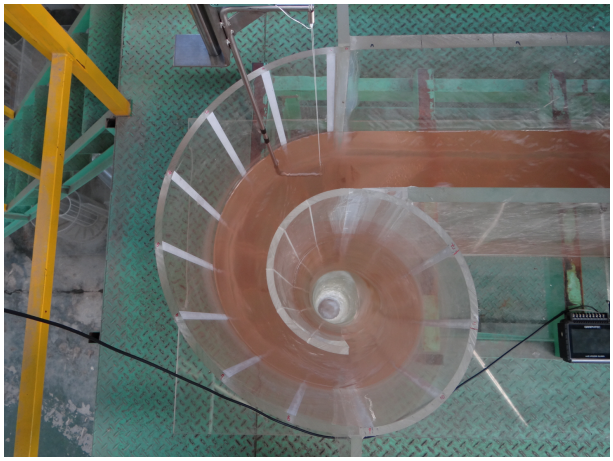

(c) Top view of the vertical shaft with the spiral intake structure

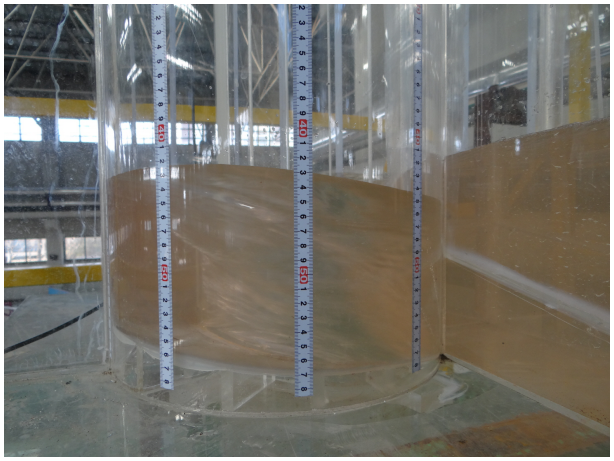

(d) Tape rulers attached to the outer wall of the vertical shaft to measure water surface elevations

Appendix 2 Photographs of the model vortex drop inlet used in the experiments